

Supplementary Materials: Effect of the Chemical Composition of Simulated Body Fluids on Aerogel-Based Bioactive Composites

Enikő Győri, István Fábián, and István Lázár

1. Appearance of the Silica Aerogel-Based Composites

Figure S1 shows the aerogels (the control sample (left) containing only cellulose, the four barrels (right) containing tricalcium phosphate, hydroxyapatite and cellulose as additives) after the supercritical drying process. As shown, the additives were distributed homogeneously in the samples by our patented process. [1] The height of the barrels was approximately 6 cm, the diameter was at around 2.2 cm. As a result of the heat treatment after the supercritical drying, the cylinders sintered to circa 40% of the original size. The samples were cut from the corresponding monolithic block with a diamond blade cutter.

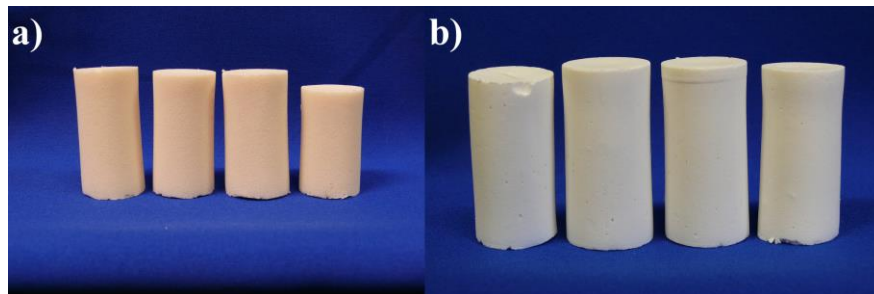


Figure S1. Pictures of the obtained aerogels after the supercritical drying process. The control samples (a), contained only cellulose as additive. The rightward barrels (b) contained cellulose, tricalcium phosphate and hydroxyapatite. The additives are distributed homogeneously in both samples.

2. Chemical Composition of the Prepared Simulated Body Fluids

The table below shows the chemical compositions of the applied simulated body fluids. The two biocide agents were used to keep the solutions sterile otherwise bacteria appeared on the surfaces of the samples (Figure S2). The size and the shape of the microbes are similar to some common bacteria, like *Pseudomonas aeruginosa* or *Escherichia coli*. [2,3]

Table S1. Chemical compositions of the prepared simulated body fluids.

Solution "A" (100.0 mL)	SBF1 <i>m</i> (g)	SBF2 <i>m</i> (g)	SBF3 <i>m</i> (g)	SBF4 <i>m</i> (g)
HCl	0.0366	0.0362	0.011	0.0232
NaCl	1.5989	1.599	1.5991	1.3327
KCl	0.0449	0.045	0.044	0.0449
MgCl ₂ ·6H ₂ O	0.061	0.061	0.0616	0.0609
CaCl ₂	0.0556	0.0279	0.1112	0.1115
Gentamicin	0.0053	0.005	0.0048	0.0051
Kanamycine	0.0103	0.0103	0.0105	0.0103
TRIS stock solution (mL)	5.0	5.0	5.0	5.0
Amino acid stock solution (mL)	0.0	0.0	1.0	1.0
Bovine serum albumin	0.0	0.0	4.0036	4.006

Solution "B" (100.0 mL)	SBF1 m (g)	SBF2 m (g)	SBF3 m (g)	SBF4 m (g)
Na ₂ SO ₄	0.0145	0.0146	0.0143	0.0142
NaHCO ₃	0.0715	0.0704	0.0706	0.4537
K ₂ HPO ₄	0.0356	0.0348	0.035	0.035
Gentamicin	0.0051	0.005	0.0048	0.0048
Kanamycine	0.0101	0.0097	0.0102	0.0099
TRIS Stock Solution (mL)	5.0	5.0	5.0	5.0
Amino Acid Stok Solution (mL)	0.0	0.0	1.0	1.0
Bovine Serum Albumin	0.0	0.0	4.0033	4.0064

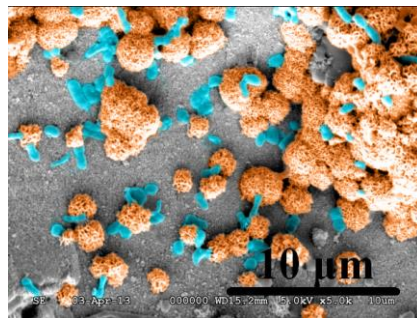


Figure S2. Scanning electron micrograph of an infected sample from an earlier experiment. Due to the non-sterile conditions, unicellular microbes—for example *Pseudomonas aeruginosa* or *Escherichia coli* (blue coloured)—appeared on the surface of the sample.

3. Nitrogen Adsorption/Desorption Isotherms of the Studied Samples

The isotherms of the studied samples are shown in Figure S3. The hysteresis loop, which indicates mesoporous structure, appears in the cases of all the four samples. Measurements of the samples sintered at high temperatures, confirmed that the amount of the adsorbed nitrogen decreased significantly, which means that the specific surface areas and the pore diameters are smaller. Although the porosity of the samples are considerably smaller that of the samples calcined only at 500 °C, the heat treatment at higher temperatures is crucial to obtain the appropriate mechanical strength. Nevertheless, even after sintering the samples at 1100 °C, they have porous structure.

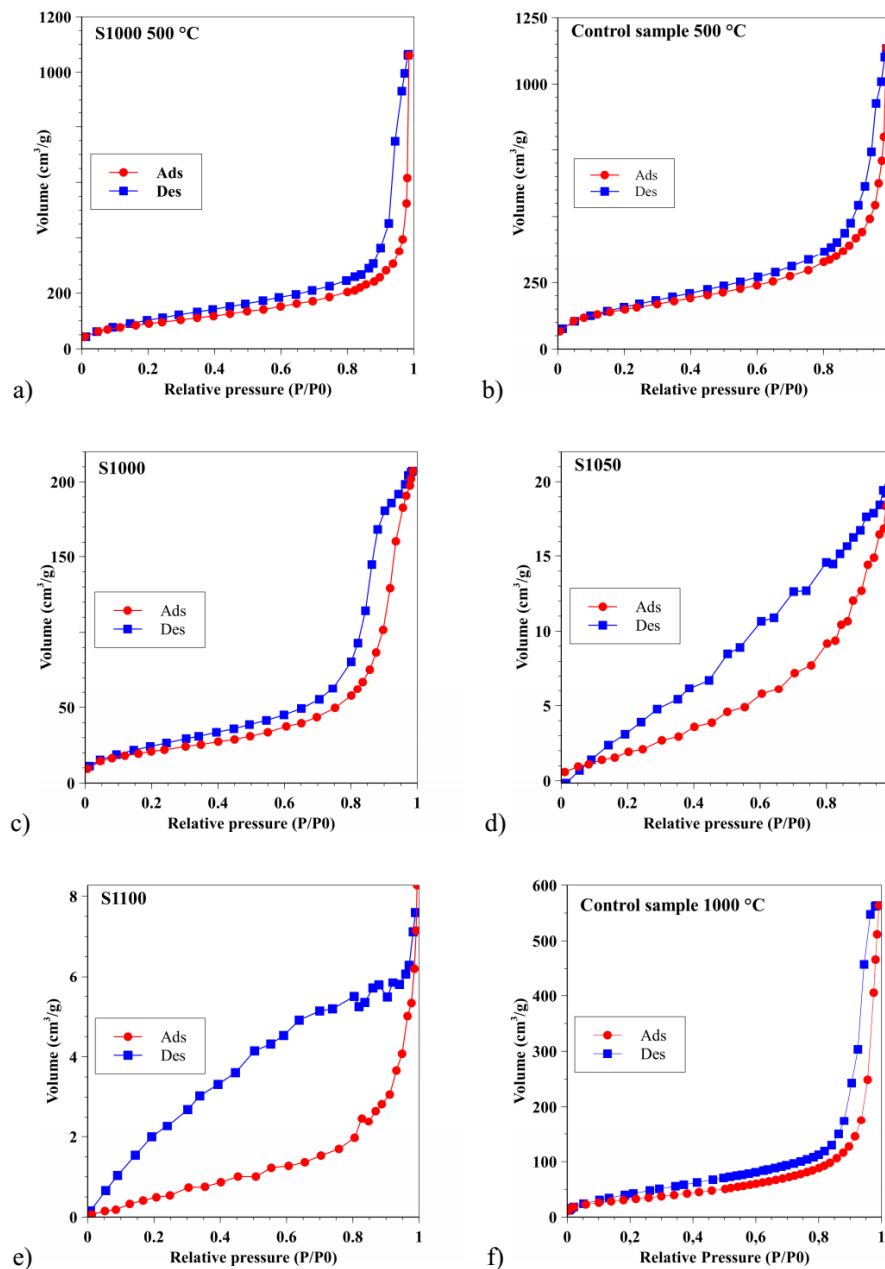


Figure S3. Nitrogen adsorption-desorption isotherms of the studied samples. The samples sintered at 500 °C adsorbed great amount of nitrogen ((a) and (b)), while with the increasing sintering temperature the volume of the adsorbed gas decreases progressively ((c) and (d)). The samples possessed porous structure even after sintering at 1100 °C (e), although both the specific surface area and the pore diameter decreased significantly. The control sample (f) did not contain any additive, that is why it adsorbed more nitrogen gas, that is, it had greater specific surface area than the sample S1000 sintered at the same temperature.

The scanning electron micrographs below (Figure S4) are recorded in an earlier experiment. The samples contained only β -tricalcium phosphate as additive. One sample was sintered at 1050 °C (left), the other at 1100 °C (right). After soaking them in simulated body fluid for fourteen days, a hydroxyapatite layer formed on the surfaces of both samples. In the present work, the samples sintered at the same temperature did not show hydroxyapatite layer formation ability. The reason for the difference is the chemical composition of the samples. Because of the basic characteristic of the β -tricalcium phosphate, the pH of the solution can drift to higher values, which can cause spontaneous hydroxyapatite deposition on the surfaces of samples.

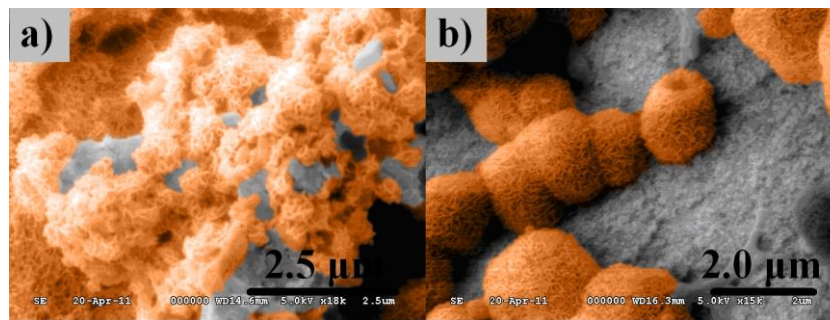


Figure S4. Scanning electron micrographs of aerogel bioceramic samples containing calcium-phosphate. The samples, sintered at 1050 °C (a) and 1100 °C (b), were soaked in simulated body fluid for two weeks. Hydroxyapatite with the typical cauliflower like structures (orange coloured) appeared on the surfaces of both samples. SEM EDX identification of the surface deposit is shown in Figure S8 and Figure S9.

4. Biocompatibility of the Samples Soaked in the Improved Simulated Body Fluids

Figure S5 shows the scanning electron micrographs of the samples treated in the modified simulated body fluids. The studied materials did not show hydroxyapatite formation ability in these fluids for several reasons.

In the case of SBF2 (Figure S5), the calcium ion concentration was only 1.26 mmol/L, which is the same as the free calcium concentration in the blood plasma. By reducing the calcium ion concentration to the half, the solution was not supersaturated and the nucleation did not occur.

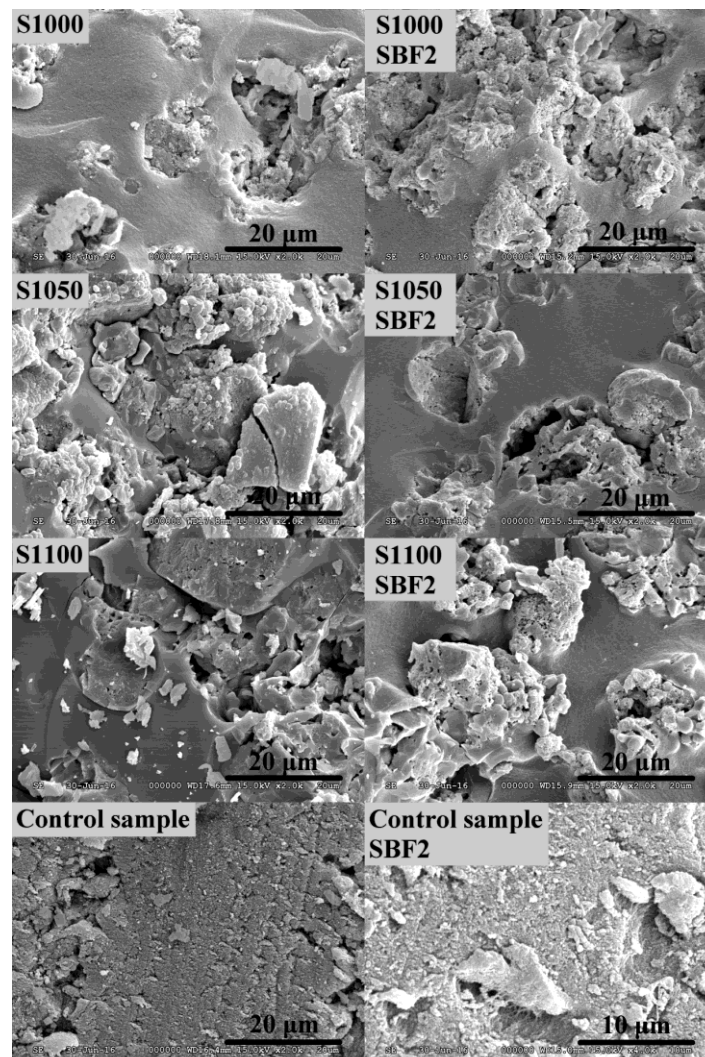


Figure S5. SEM micrographs of the samples soaked in SBF2. Due to the low effective calcium ion concentration, there was no hydroxyapatite deposition after 14 days.

SBF3 contained serum albumin and amino acids. Because of the presence of these compounds, the nucleation did not start in fourteen days, since the solution was not supersaturated. Although the calcium ion concentration was increased to 5.0 mmol/L, the albumin acted like a buffer so the free calcium ion concentration was not enough for calcium phosphate precipitation. The SEM micrographs of the samples are shown in Figure S6.

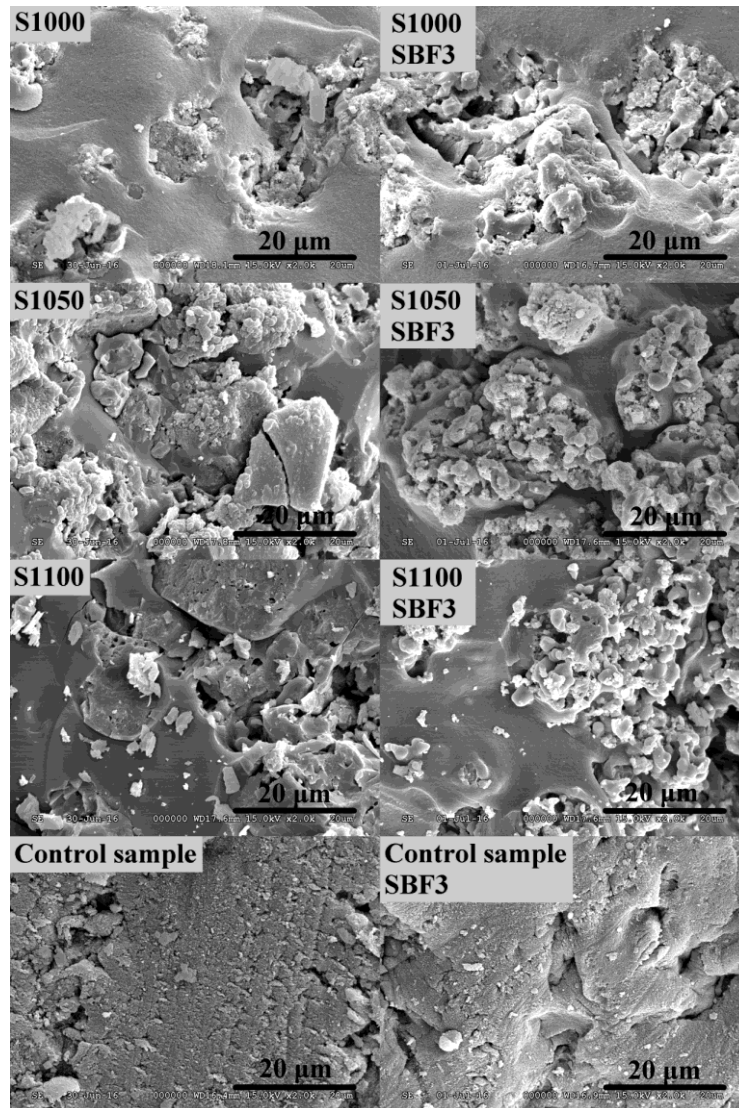


Figure S6. The SEM micrographs of the samples treated in SBF3. Due to the calcium complex formation property of serum albumin and the amino acids, there was no hydroxyapatite precipitation after two weeks.

The studied materials did not show hydroxyapatite formation ability in SBF4 either, because of the reasons mentioned above. The chemical composition of this solution was the same as that of SBF3, the only different was the concentration of HCO_3^- ion. It was increased to 27 mmol/L, which is the physiological concentration in the blood plasma. According to the scanning electron micrographs of the samples (Figure S7), we could not detect any positive or negative effect of the increased concentration.

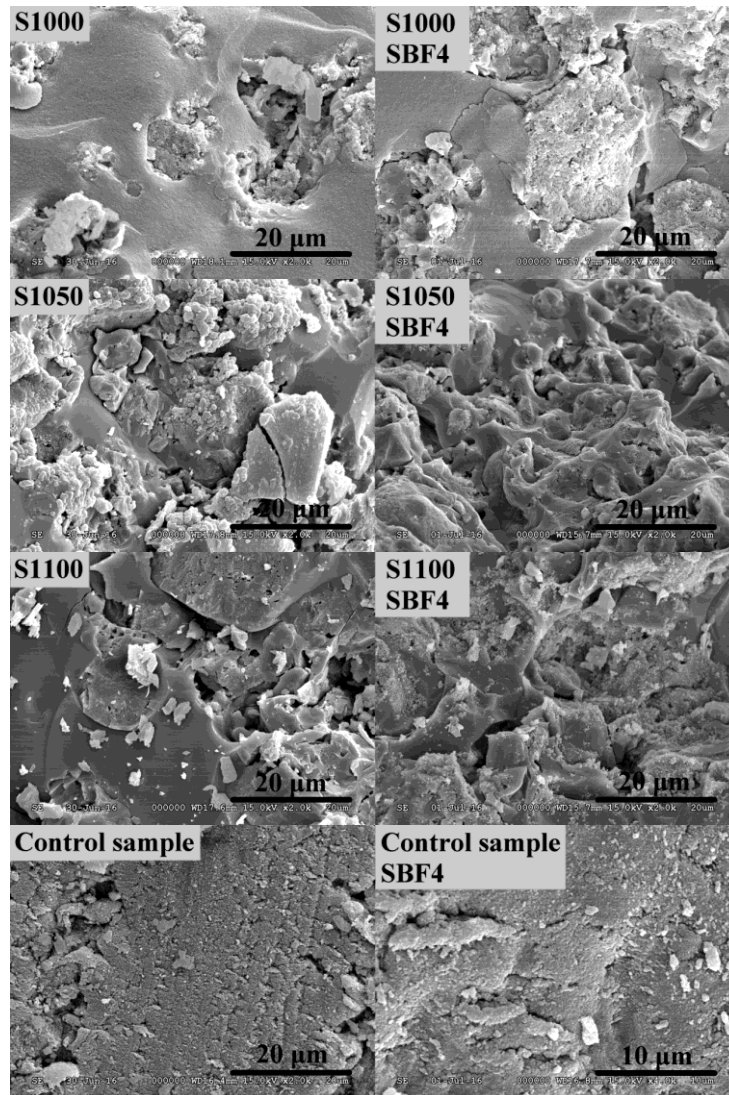


Figure S7. The SEM micrographs of the samples treated in SBF4. There was no hydroxyapatite deposition after fourteen days. The reason of this is the same as in case of SBF3, the albumin acted like a buffer and decreased the free calcium ion concentration. Thereby the solution was not supersaturated, the nucleation did not occur.

5. Identification of surface deposits

Surface deposits were identified by EDX spectroscopy at 15 kV voltage. Accumulated spectra were received from a 250 × 250 nm² sized and gold-sputtered area.

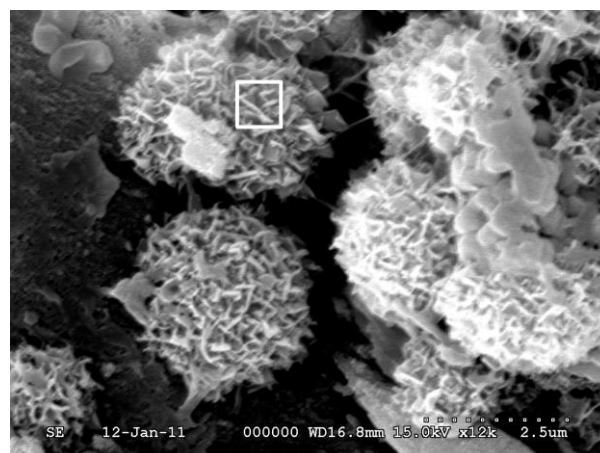


Figure S8. SEM picture of HA surface deposits on an aerogel-based biocomposite material formed in the original Kokubo’s simulated body fluid. White rectangle indicate placement of EDX beam. Spectra recorded for the area is given in Figure S9.

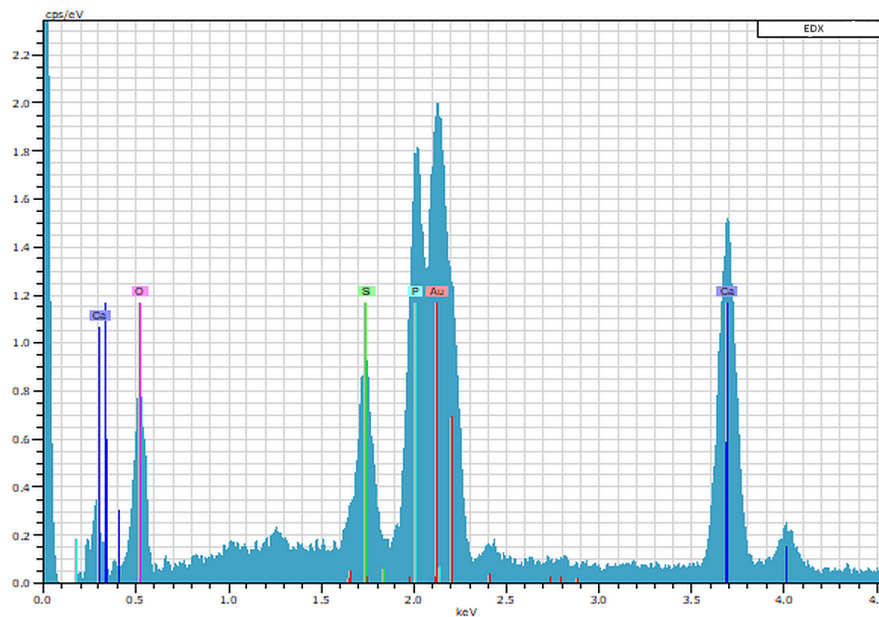


Figure S9. EDX spectrum of the surface deposit area indicted by a white rectangle in Figure S8. Ca and P peaks are characteristic and intense, while Si peak is relatively low. The intensity of silicon peak is variable in such samples in general, as the base silica aerogel layer is also excited.

6. Fine Structure and High Temperature Behaviour

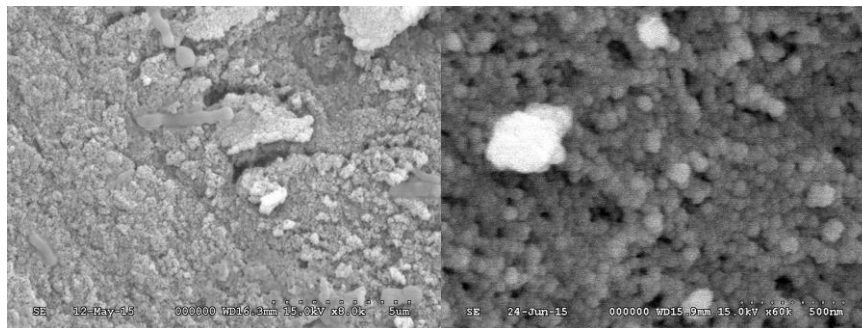


Figure S10. SEM picture of the silica aerogel matrix of artificial bone substitute materials in 8k and 64k magnification. Mesoporous nanostructure and overlapping 50-70 nm secondary globuli are shown in the right picture. The porous fine structure clearly demonstrates the basic difference between aerogel-based and traditional ceramic-based bioactive artificial bone substitute materials.

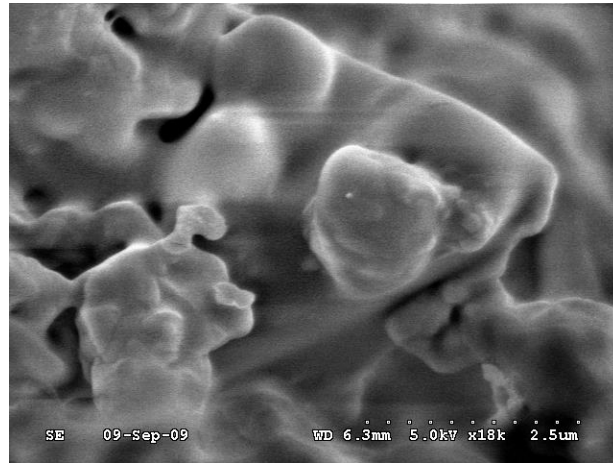


Figure S11. SEM picture indicates that the high temperature (1200 °C) viscous flow of silica aerogel that covers the entire surface of HA and TCP particles in the composite material.

References

1. Lázár, I.; Fábíán, I. Method for the preparation of composite silica alcogels, aerogels and xerogels, apparatus for carrying out the method continuously, and novel composite silica alcogels, aerogels and xerogels. Available online: https://worldwide.espacenet.com/publicationDetails/originalDocument?CC=WO&NR=2013061104A2&KC=A2&FT=D&ND=3&date=20130502&DB=EPODOC&locale=en_EP (accessed on 17 November 2016).
2. Deligianni, E.; Pattison, S.; Berrar, D.; Terman, N. G.; Haylock, R. W.; Moore, J. E.; Elborn, S. J.; Dooley, J. S. *Pseudomonas aeruginosa* Cystic Fibrosis isolates of similar RAPD genotype exhibit diversity in biofilm forming ability in vitro. *BMC Microbiol.* **2010**, *10*, 38, doi:10.1186/1471-2180-10-38.
3. Nath, A.; Joshi, S. R. Ultrastructural effect on mastitis pathogens by extract of endophytic fungi associated with ethnoveterinary plant, *Hibiscus sabdariffa* L. *J. Microsc. Ultrastruct.* **2015**, *3*, 38–43, doi:10.1016/j.jmau.2014.10.001.